Experimental investigation of smoothing by spectral dispersion

Sean P. Regan, John A. Marozas, John H. Kelly, Thomas R. Boehly, William R. Donaldson, Paul A. Jaanimagi, Robert L. Keck, Terrance J. Kessler, David D. Meyerhofer, Wolf Seka, Stanley Skupsky, and Vladimir A. Smalyuk

Laboratory for Laser Energetics, University of Rochester, 250 East River Road, Rochester, New York 14623-1299

Received October 25, 1999; revised manuscript received May 15, 2000

Measurements of smoothing rates for smoothing by spectral dispersion (SSD) of high-power, solid-state laser beams used for inertial confinement fusion (ICF) research are reported. Smoothing rates were obtained from the intensity distributions of equivalent target plane images for laser pulses of varying duration. Simulations of the experimental data with the known properties of the phase plates and the frequency modulators are in good agreement with the experimental data. These results inspire confidence in extrapolating to higher bandwidths and other SSD configurations that may be suitable for ICF experiments and ultimately for direct-drive laser-fusion ignition. © 2000 Optical Society of America [S0740-3224(00)01909-3]

OCIS codes: 350.2660, 140.3580, 140.3610, 030.6140, 030.6600.

1. INTRODUCTION

In the direct-drive approach to inertial confinement fusion (ICF), capsules are irradiated directly by a large number of symmetrically arranged laser beams.[1,2] Nonuniformities in the laser irradiation may seed the Rayleigh–Taylor hydrodynamic instability, which degrades target performance[3]; therefore a combination of beam-smoothing techniques is employed to achieve the high irradiation uniformity required for direct-drive laser-fusion experiments. These techniques, which include two-dimensional smoothing by spectral dispersion (2-D SSD),[4–6] distributed phase plates,[7,8] polarization smoothing,[9–11] and multiple-beam overlap, will also be implemented on the 1.8-MJ, 351-nm, 192-beam National Ignition Facility,[12] which is currently under construction at the Lawrence Livermore National Laboratory. Direct-drive laser fusion requires a high degree of laser-irradiation uniformity on target: The rms irradiation nonuniformity must be below 1% when the laser intensity has been averaged over a few hundred picoseconds.[2,5]

Characterization of the laser-irradiation nonuniformity is essential for ICF research, since the efficiency with which the nonuniformities in the laser-irradiation imprint target mass perturbations (i.e., laser imprint) depends on the early-time intensity history and on the spatial wavelength of the nonuniformity.[13] The strategy of 2-D SSD with phase plates, which is the preferred mechanism for reducing laser-beam irradiation nonuniformity in glass lasers, is to vary the interference (speckle) pattern of the phase plate on a time scale that is short compared with the characteristic hydrodynamic response time of the target (i.e., imprinting time). (An alternative technique, induced spatial incoherence, has been developed for KrF lasers.[14]) Predictions show that 2-D SSD smoothing with $\Delta\nu_{\mathrm{UV}} \approx 1$ THz will smooth the spherical-harmonic modes of $l = 20–150$ to acceptable levels for ICF.[5] The bandwidth on OMEGA[15] will be increased from 0.2 to 1 THz during this year, which will decrease the smoothing time by a factor of $\sqrt{5}$.

In this research the temporal rate of beam smoothing produced by 2-D SSD with the current bandwidth of $\Delta\nu_{\mathrm{UV}} \approx 0.2$ THz is quantified by analysis of measured UV equivalent-target-plane (UVETP) images of a single OMEGA laser beam. Sections 2–4 describe (1) laser-beam smoothing with 2-D SSD and phase plates, (2) 2-D SSD model calculations, and (3) the diagnostic used to record UVETP images of laser pulses with constant peak power and varying duration (100 ps to 3.5 ns). Power spectra calculated from the measured UVETP images along with the measured smoothing rate of 2-D SSD are presented and compared with theoretical predictions in Section 5. This study shows that the theoretical predictions of 2-D SSD laser-beam smoothing are in excellent agreement with the measured temporal smoothing rates.

2. BACKGROUND

Smoothing of laser beams with SSD was described in Ref. 4. On OMEGA the phase plates are placed before the focusing lens and produce far-field spots with highly reproducible spatial intensity envelopes and speckle distributions. We achieve smoothing by spectral dispersion by frequency modulating the phase of a laser beam, wavelength dispersing the beam, and passing it through a phase plate so that the spectral components are separated in the target plane by at least one-half the beam's diffraction-limited width. The reduction in laser-irradiation nonuniformity is wavelength dependent. The longest wavelength of nonuniformity that can be smoothed by SSD is twice the maximum spatial shift $S_{\max} = F\Delta\theta$ of the speckle pattern that can be produced by the laser, where $\Delta\theta$ is the angular spread of the wavelength-dispersed light propagating through the laser and F is the focal length of the OMEGA lens. (The ulti-

0740-3224/2000/091483-07$15.00

mate limit of S is given by the maximum allowable angular spread in the spatial filter in the laser system.) Thus spherical-harmonic modes of nonuniformity down to $l_{\mathrm{cut}} = 2\pi R/(2S_{\max})$, where R is the target radius, can be smoothed with 2-D SSD.[5] Spherical targets on OMEGA have $R = 500\ \mu\mathrm{m}$, and the present 2-D SSD system has $S_{\max} = 100\ \mu\mathrm{m}$; hence $l_{\mathrm{cut}} = 16$.

3. MODEL CALCULATIONS

The time-integrated far field is calculated by temporal integration of the modulus squared of a two-dimensional spatial Fourier transform of the UV near field. The complex-valued electric field that describes the UV near field can be written as

$$E(x, y, t) \equiv E_0(x, y, t)\exp[i\phi_{\text{2-D SSD}}(x, y, t)] \times \exp[i\phi_B(x, y, t)]\exp[i\phi_{\mathrm{DPP}}(x, y)], \quad (1)$$

where $E_0(x, y, t)$ defines the temporal and the spatial beam shapes, $\phi_{\text{2-D SSD}}(x, y, t)$ is the 2-D SSD phase contribution, $\phi_B(x, y, t)$ is the intensity-dependent phase contribution of the B integral,[16] and $\phi_{\mathrm{DPP}}(x, y)$ is the static distributed phase-plate contribution, which depends on the particular phase-plate design.

The spatially and temporally varying phase that is due to 2-D SSD is[17]

$$\phi_{\text{2-D SSD}}(x, y, t) \equiv 3\delta_{Mx}\sin[\omega_{Mx}(t + \xi_x x)] + 3\delta_{My}\sin[\omega_{My}(t + \xi_y y)], \quad (2)$$

where the x and the y subscripts denote the two smoothing dimensions, $\delta_{Mx,y}$ is the modulation depth, $\nu_{Mx,y} = \omega_{Mx,y}/2\pi$ is the rf modulation frequency, and $\xi_{x,y}$ is the angular grating dispersion. The factor of 3 in Eq. (2) indicates that the electric field has undergone frequency tripling from the IR to the UV. The 2-D SSD system parameters on OMEGA for the UVETP measurements are $\delta_{Mx} = 5.12$, $\nu_{Mx} \equiv 3.31$ GHz, $\xi_x = 1.11$ ns/m, $\Delta\lambda_{Mx} = 1.25$ Å, $\delta_{My} = 7.89$, $\nu_{My} \equiv 3.0$ GHz, $\xi_y = 1.11$ ns/m, and $\Delta\lambda_{My} = 1.75$ Å, assuming a nominal beam diameter of 27.5 cm. The modulation depths and the bandwidths are given for the IR. The maximum angular spread $\Delta\theta$ is given by $\Delta\theta = \xi(c/\lambda)\Delta\lambda$, where c is the speed of light and $\lambda = 1053$ nm. Cases without frequency modulation are modeled by means of setting modulation depths equal to zero, i.e., $\delta_{Mx} = 0$ and $\delta_{My} = 0$.

Our simulations indicate that B-integral effects are negligible for all cases except when the frequency modulation is turned off.

4. ULTRAVIOLET EQUIVALENT-TARGET-PLANE DIAGNOSTIC

The layout of the diagnostic used to acquire the UVETP images of a single OMEGA beam is shown in Fig. 1. Time-integrated UVETP images were recorded with a CCD camera. All the measurements presented in this paper exploit the low noise level and the large dynamic range of the CCD to extract power spectra from the UVETP images with negligible noise levels. The UV-sensitive CCD camera is a backthinned SITe 003B chip in a Photometrics Series 300 camera.[18] The sensor has an array of 1024×1024 photosensitive elements with a pixel size of $24\ \mu\mathrm{m} \times 24\ \mu\mathrm{m}$. Two pixels of the CCD camera correspond to $\sim 1\ \mu\mathrm{m}$ in the target plane, which is approximately five times the f-number-limited spatial frequency $f_0 \equiv D/\lambda F$, where D is the beam diameter of the OMEGA lens and $\lambda = 351$ nm.

A full-aperture optical wedge in one of the 60 laser beams (BL-19) directs 4% of the laser light to an OMEGA focusing lens (see Fig. 1). The phase plate is placed directly in front of the lens, mimicking the target–beam configuration. The beam is brought through focus in a vacuum tube, down collimated with a doublet lens, brought to focus with a 2-m lens, and relayed to the CCD camera with the final lens. The beam intensity is reduced with three 4% reflections (not shown in Fig. 1) and the fifth-order reflection of a rattle plate (consisting of two surfaces with $R = 70\%$ per surface). The optical background is reduced to negligible levels with a light shield surrounding the CCD optics and the CCD camera. The light levels incident on the CCD are optimized by means of attenuating the beam with a neutral-density filter that is placed after the final lens. Background-visible and IR signals are blocked with broadband UG1 (Ref. 19) and U360 (Ref. 20) UV bandpass filters mounted in front of the CCD camera. Compared with the laser spot size on target the UVETP image on the CCD camera is magnified by a factor of ~ 42.

Small-scale and whole-beam B-integral effects were found to provide smoothing of beams without frequency modulation. (The detailed analysis of beams without frequency modulation will be presented in a separate publication.) A UVETP image of a laser pulse with zero accumulated B integral (B integral < 1.0 rad in the UV) and no frequency modulation was measured to quantify the amount of beam smoothing that is due to the B integral at higher laser powers. The power spectrum is the azimuthal sum at each spatial frequency of the square of the Fourier amplitudes, and the Fourier transform is performed with a Hamming window applied to the data. The power spectrum is normalized to the total power, and the single-beam irradiation nonuniformity σ_{rms} is defined as the square root of the ratio of the power in the high frequencies (i.e., $k \geqslant 0.04\ \mu\mathrm{m}^{-1}$ in the OMEGA target plane) to the power in the low frequencies (i.e., $k < 0.04\ \mu\mathrm{m}^{-1}$). The highest (cutoff) wave number $k = 2.24\ \mu\mathrm{m}^{-1}$ corresponds to the f-number-limited spatial frequency. A spectrum for a zero-B-integral laser pulse without frequency modulation is shown in Fig. 2, and its irradiation nonuniformity, $\sigma_{\mathrm{rms}} = 93.4\%$, is the

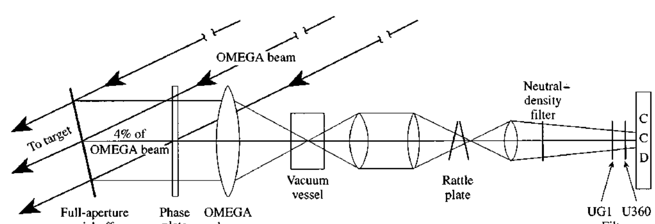

Fig. 1. Schematic of the UVETP diagnostic. The on-target spot size is magnified by $M = 42$ on the CCD camera.

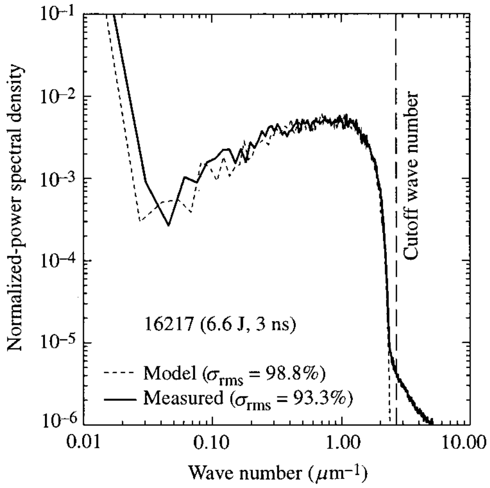

Fig. 2. Power spectra obtained from a UVETP image of a laser pulse with zero accumulated B integral (B integral < 1.0 rad in the UV) without frequency modulation. The power spectrum is the azimuthal sum at each frequency of the square of the Fourier amplitudes, and the cutoff wave number corresponds to the f-number-limited spatial frequency. The power spectra are normalized to the total power, and the $\sigma_{\rm rms}$ is defined as the square root of the ratio of the power in the high frequencies (i.e., $k \geq 0.04\ \mu\text{m}^{-1}$ in the OMEGA target plane) to the power in the low frequencies (i.e., $k < 0.04\ \mu\text{m}^{-1}$). Solid and dashed curves represent measured and modeled power spectra, respectively. The predicted speckle structure shows excellent agreement with the measurement; hence the zero accumulated B-integral shot serves as a calibration that demonstrates the capability of the UVETP diagnostic to resolve fully individual speckles.

highest measured under any condition and is near the 100% value expected from theory.

The theoretical power spectrum simulated with the time-dependent code (described in Section 3) is also shown in Fig. 2 and includes the spatiotemporal near-field irradiance and small-scale and whole-beam B-integral effects. The higher value of $\sigma_{\rm rms}$ predicted by the model is caused by the discrepancy between the model and the measurement in the low wave numbers (see Fig. 2). Nevertheless, the predicted speckle structure shows excellent agreement with the measurement; hence the zero accumulated B-integral shot serves as a calibration that demonstrates the capability of the UVETP diagnostic to measure highly modulated spatial-intensity profiles of pulses with no frequency modulation.

The envelope and the speckle were separated at wave number 0.04 μm^{-1} in the calculation of $\sigma_{\rm rms}$ for two reasons. First, virtually all the envelope power is contained in the first three terms of the Fourier transform, which have wave numbers $k < 0.04\ \mu\text{m}^{-1}$; therefore inclusion of additional terms in this sum increases the envelope power by insignificant amounts. Second, the smallest wave number of nonuniformity that can be smoothed on OMEGA with 0.2-THz 2-D SSD falls between the third and the fourth terms of the Fourier transform with wave numbers of 0.031 and 0.046 μm^{-1}. Therefore the terms of the Fourier transform from the fourth term with $k \geq 0.04\ \mu\text{m}^{-1}$ to the cutoff wave number $k = 2.24\ \mu\text{m}^{-1}$ contain all the wave numbers that 2-D SSD can smooth.

5. EXPERIMENTAL RESULTS AND ANALYSIS

Measured UVETP images of 3.5-ns square laser pulses without frequency modulation and with 2-D SSD are presented in Figs. 3(a) and 3(b), respectively. These images qualitatively illustrate the effect of laser-beam smoothing with 2-D SSD. The images with 2-D SSD show a smooth spatial intensity envelope [see single-pixel lineout overplotted on image in Fig. 3(b)], whereas the pulses without frequency modulation have a highly modulated spatial intensity profile [see single-pixel lineout overplotted on image in Fig. 3(a)]. The spatial resolution and overall detector size of the CCD restrict the UVETP measurement to slightly more than one-half the laser-beam profile. As seen in Fig. 3, the laser beam is centered nominally on the photodetector, and 585 μm of the 950-μm (defined as the 95% enclosed energy contour) laser spot is sampled. Alignment constraints for the compilation of laser shots under consideration restrict the analysis to ~410 μm of the 950-μm laser spot.

The temporal rate of 2-D SSD smoothing is deduced from the power spectra of the measured UVETP images of laser pulses with constant peak power and pulse lengths ranging from 100 ps to 3.5 ns. Power spectra calculated from measured UVETP images of (a) 100-ps and (b) 3-ns laser pulses smoothed with 2-D SSD are presented in Fig. 4. The time-dependent nature of 2-D SSD smoothing is evident in the measured results with lower measured values of $\sigma_{\rm rms}$ for the longer pulse lengths. As pointed out in Section 4 for the $\sigma_{\rm rms}$ calculation, virtually all the envelope power has wave numbers $k < 0.04\ \mu\text{m}^{-1}$. Nevertheless, the spatial-intensity envelope influences the shape of the low-wave-number ($k < 0.07\ \mu\text{m}^{-1}$) power spectrum. In contrast to the contribution of power that is due to laser speckle in this low-wave-number range, which cannot be reduced, the amount of power in this range that is due to the spatial intensity envelope can be controlled with phase-plate design. The UVETP diagnostic was configured with a phase plate that produced a

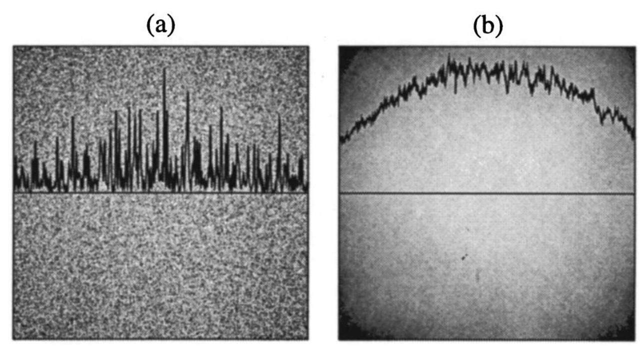

Fig. 3. Measured UVETP images of 3.5-ns square laser pulses (a) without frequency modulation and (b) with 2-D SSD at $\Delta\nu_{\rm UV} \approx 0.2$ THz. As demonstrated with the single-pixel lineout through the center of the beam, the laser pulse with 2-D SSD has a smooth spatial intensity envelope, whereas the pulse without frequency modulation has a highly modulated spatial intensity profile. The spatial resolution and the overall detector size of the CCD restrict the UVETP measurement to slightly more than one-half the laser-beam profile. The laser beam is centered nominally on the photodetector, and 585 μm of the 950-μm laser spot (defined as the 95% enclosed energy contour) is sampled.

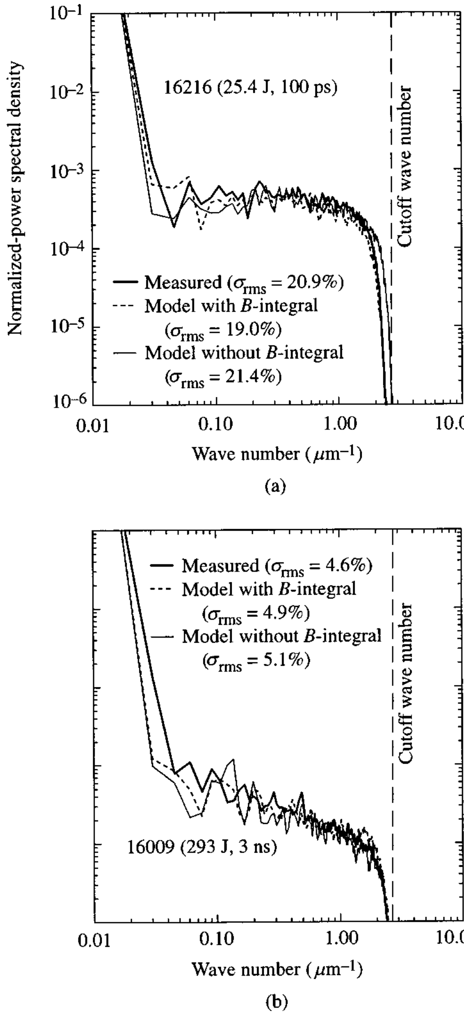

Fig. 4. Power spectra calculated from UVETP images of (a) 100-ps and (b) 3-ns laser pulses with 2-D SSD. Thick solid curve, measured power spectrum. Dashed curve, time-dependent simulation that includes both the spatiotemporal behavior of the near-field irradiance and small-scale and whole-beam B-integral effects. Thin solid curve, time-dependent model neglecting B-integral effects. Both models are in agreement with the measured results, and B-integral effects are negligible for all cases except for pulses without frequency modulation.

far-field spot with a super-Gaussian spatial intensity envelope $[I \sim \exp(r/r_0)^{2.5}]$ for these pulses.

The 2-D SSD power spectra simulated with the time-dependent code (described in Section 3) with and without B-integral effects are plotted in Fig. 4. The B-integral effects are completely negligible as shown in this figure. The excellent agreement between the simulated power spectra and the measured spectra is clearly apparent in Fig. 4.

The measured temporal rate of 2-D SSD smoothing is shown in Fig. 5, which shows a compilation of data from more than 150 laser shots that clearly demonstrates the decrease in the measured σ_{rms} with increasing pulse length. Statistical error bars are smaller than the symbols. The 3.5-ns pulse has the lowest measured $\sigma_{\mathrm{rms}} = 5.3\%$. The measurement of the laser-irradiation nonuniformity for the 3.5-ns pulses without frequency modulation is also presented for comparison. The thin solid curve is the time-integrated simulation of the single-beam irradiation nonuniformity σ_{rms} that neglects the B-integral effects and assumes a static near field with a uniform irradiance. The simulation is in agreement with the measured results (circles). The thick solid curve in Fig. 5 represents model predictions for σ_{rms},

$$\sigma_{\mathrm{rms}} = \left[\sigma_0{}^2\left(\frac{t_c}{t + t_c}\right) + \sigma_{\mathrm{asymp}}{}^2\right]^{1/2}, \tag{3}$$

where $t_c = 1/\Delta\nu_{\mathrm{UV}} = 5$ ps is the coherence time, $\Delta\nu_{\mathrm{UV}} = 0.2$ THz is the UV bandwidth, t is the averaging time (i.e., pulse length), σ_0 is the initial laser nonuniformity, and σ_{asymp} is the asymptotic level of 2-D SSD smoothing taken from Eq. (8) of Ref. 21. This prediction adds the asymptotic levels of smoothing in quadrature to the model given in Ref. 14. The dashed curve in Fig. 5 is a plot of Eq. (3) with σ_{asymp} set to zero. The effective $\Delta\nu_{\mathrm{UV}}$ was independently measured with a time-integrated UV spectrometer for the compilation of laser shots under consideration to be 0.2 THz with a standard deviation of 0.02 THz. The deviation of the thick solid curve from the dashed curve near 1 ns signifies that the beam smoothing is approaching its asymptotic limit. The asymptotic behavior can be observed in the measured values of σ_{rms}.

The dependence of the rate of smoothing on the wave number k is examined in Fig. 6, where σ_{rms} is plotted as a function of pulse length for the spectral wavelength ranges of $\lambda = 20$-, $\lambda = 30$-, $\lambda = 60$-, and $\lambda = 150$-μm wavelengths, corresponding to $k = 0.31\ \mu\mathrm{m}^{-1}$, $k = 0.21\ \mu\mathrm{m}^{-1}$, $k = 0.10\ \mu\mathrm{m}^{-1}$, and $k = 0.04\ \mu\mathrm{m}^{-1}$. Statistical error bars are again smaller than the symbols for the majority of the data. For OMEGA this corresponds to spherical-harmonic modes of $l = 20$–150, which are considered to be the most dangerous for ICF implosions.[5] Again the time-integrated 2-D SSD predictions are in

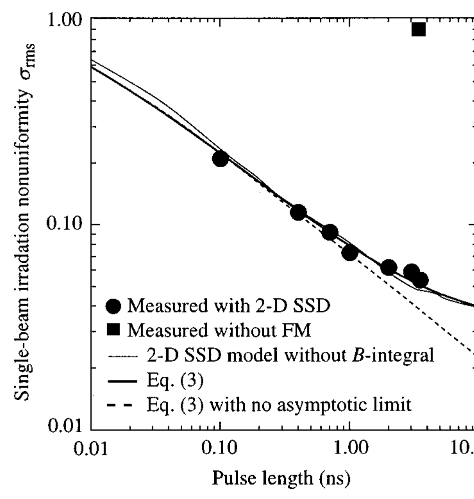

Fig. 5. Compilation of data from more than 150 laser shots demonstrates the temporal smoothing rates of 2-D SSD. Statistical error bars are smaller than the symbols. The 3.5-ns pulse has the lowest measured $\sigma_{\mathrm{rms}} = 5.3\%$. The 3.5-ns pulse without frequency modulation is shown for comparison. Thin solid curve, time-integrated simulation of the single-beam irradiation nonuniformity σ_{rms} that neglects the B-integral effects and assumes a static near field with a uniform irradiance. Thick solid curve, model predictions for σ_{rms} with Eq. (3). Dashed curve, model prediction for σ_{rms} with $\sigma_{\mathrm{asymp}} = 0$.

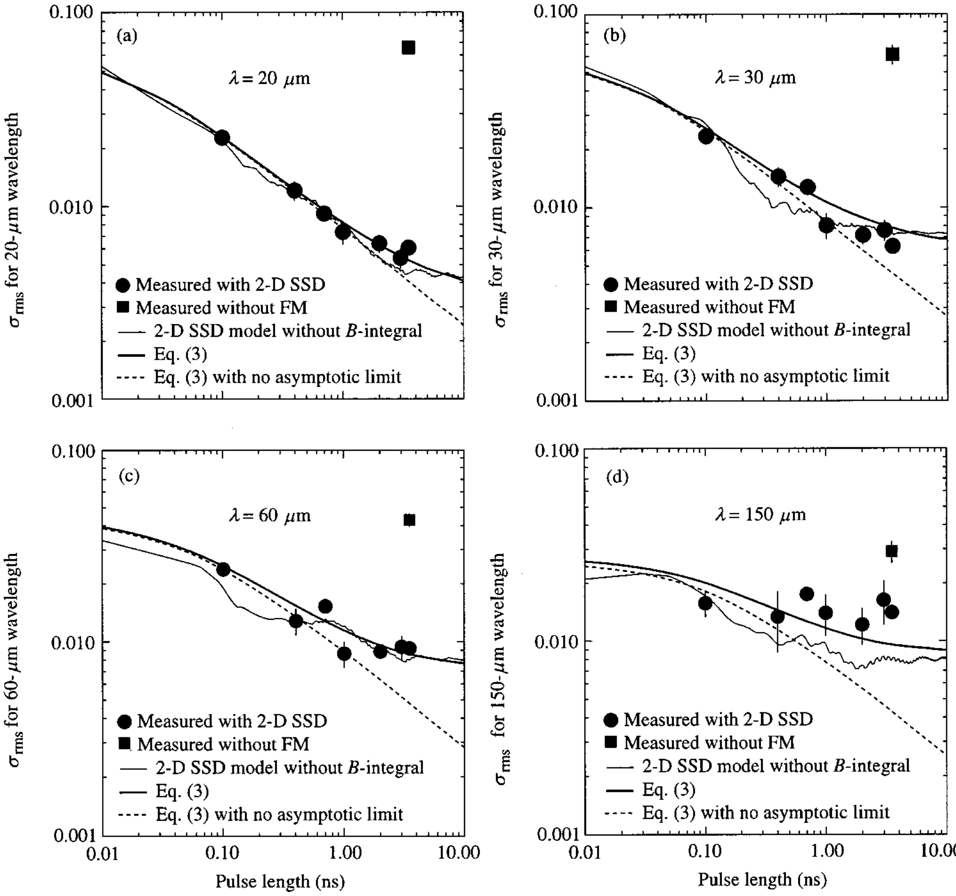

Fig. 6. Temporal smoothing rates for specific spatial wavelengths (a) λ = 20 μm (k = 0.31 μm^{-1}), (b) λ = 30 μm (k = 0.21 μm^{-1}), (c) λ = 60 μm (k = 0.10 μm^{-1}), and (d) λ = 150 μm (k = 0.04 μm^{-1}). Statistical error bars are smaller than the symbols for the majority of the data. The 2-D SSD predictions are in good agreement with the experimental observations. Thick solid curve, model predictions for σ_{rms} with Eqs. (3) and (4). Dashed curve, model prediction for $\sigma_{\text{asymp}} = 0$. Thin solid curve, predicted σ_{rms} from a 2-D SSD simulation with a static near field with a uniform irradiance and neglecting B-integral effects.

good agreement with the experimental observations (B-integral effects are negligible here, too). The data have also been fitted with Eq. (3) with the approximation based on equations in Ref. 5:

$$t_c = [\Delta \nu_{\text{UV}} \sin(k\,\delta/2)]^{-1}, \tag{4}$$

where δ is the separation between spectral modes. (For one color cycle δ corresponds to one-half a speckle width, i.e., $\delta = F\lambda/D = 2.35\ \mu\text{m}$.) In a manner similar to that in Fig. 5 the case neglecting the asymptotic behavior of Eq. (3) is also plotted in Fig. 6. We determined the initial value of the laser nonuniformity σ_0 for each spectral range by taking the average value of the measured σ_{rms} for shots without frequency modulation. The data in Fig. 6 demonstrate that the shorter wavelengths (λ = 20 μm) are smoothed more effectively than the longer wavelengths. It can also be observed that the longer-wavelength modes have higher asymptotic levels of nonuniformity than the shorter ones. Only a small amount of smoothing is observed for λ = 150-μm wavelength (corresponding to $l \approx 20$), which is in agreement with the prediction.

6. CONCLUSION

Direct-drive ICF experiments require a laser system with excellent irradiation uniformity. Two-dimensional smoothing by spectral dispersion (2-D SSD) is currently the best mechanism for reducing laser-beam nonuniformities for high-power–high-energy glass lasers. UVETP images of a single OMEGA laser beam were recorded to quantify the single-beam irradiation nonuniformity. We have determined the smoothing rate of 2-D SSD (with the current UV bandwidth of $\Delta\nu_{\text{UV}} \approx 0.2$ THz) by analyzing the power spectra of measured UVETP images of laser pulses with constant peak power and pulse lengths ranging from 100 ps to 3.5 ns. Simulated 2-D SSD power spectra and temporal smoothing rates are in excellent agreement with the experimental data and permit confident extrapolation to larger laser systems and to higher UV bandwidths.

ACKNOWLEDGMENTS

The authors appreciate the support of Sam Morse and the entire OMEGA engineering staff, especially Chris Cotton for the design of the CCD optics; Charles Kellogg for the installation of the diagnostic; and Keith Thorp, Per Adamson, Ray Huff, Matt Kamm, Dave Kuhn, and Howard Ammenheuser for the operation and alignment of the diagnostic. This study was supported by the U.S. Department of Energy (DOE) Office of Inertial Confinement Fusion under Cooperative Agreement DE-FC03-92SF19460, the University of Rochester, and the New York State Energy Research and Development Authority. The support of the DOE does not constitute an endorsement by the DOE of the views expressed in this paper.

S. P. Regan can be reached by e-mail at sreg@lle.rochester.edu.

REFERENCES

1. C. P. Verdon, "High-performance direct-drive capsule designs for the national ignition facility," Bull. Am. Phys. Soc. **38**, 2010 (1993).
2. S. E. Bodner, D. G. Colombant, J. H. Gardner, R. H. Lehmberg, S. P. Obenschain, L. Phillips, A. J. Schmitt, J. D. Sethian, R. L. McCrory, W. Seka, C. P. Verdon, J. P. Knauer, B. B. Afeyan, and H. T. Powell, "Direct-drive laser fusion: status and prospects," Phys. Plasmas **5**, 1901–1918 (1998).
3. D. K. Bradley, J. A. Delettrez, and C. P. Verdon, "Measurements of the effect of laser beam smoothing on direct-drive inertial-confinement-fusion capsule implosions," Phys. Rev. Lett. **68**, 2774–2777 (1992); J. Delettrez, D. K. Bradley, and C. P. Verdon, "The role of the Rayleigh–Taylor instability in laser-driven burnthrough experiments," Phys. Plasmas **1**, 2342–2349 (1994); J. D. Kilkenny, S. G. Glendinning, S. W. Haan, B. A. Hammel, J. D. Lindl, D. Munro, B. A. Remington, S. V. Weber, J. P. Knauer, and C. P. Vernon, "A review of the ablative stabilization of the Rayleigh–Taylor instability in regimes relevant to inertial confinement fusion," Phys. Plasmas **1**, 1379–1389 (1994); R. Epstein, "Reduction of time-averaged irradiation speckle nonuniformity in laser-driven plasmas due to target ablation," J. Appl. Phys. **82**, 2123–2139 (1997); V. A. Smalyuk, T. R. Boehly, D. K. Bradley, V. N. Goncharov, J. A. Delettrez, J. P. Knauer, D. D. Meyerhofer, D. Oron, and D. Shvarts, "Saturation of the Rayleigh–Taylor growth of broad-bandwidth laser-imposed nonuniformities in planar targets," Phys. Rev. Lett. **81**, 5342–5345 (1998).
4. S. Skupsky, R. W. Short, T. Kessler, R. S. Craxton, S. Letzring, and J. M. Soures, "Improved laser-beam uniformity using the angular dispersion of frequency-modulated light," J. Appl. Phys. **66**, 3456–3462 (1989).
5. "Two-dimensional SSD on OMEGA," Laboratory for Laser Energetics (LLE) Review 69, available as NTIS document DOE/SF/19460-152 (National Technical Information Service, Springfield, Va., 1996), pp. 1–10; S. Skupsky and R. S. Craxton, "Irradiation uniformity for high-compression laser-fusion experiments," Phys. Plasmas **6**, 2157–2163 (1999).
6. J. E. Rothenberg, "Comparison of beam-smoothing methods for direct-drive inertial confinement fusion," J. Opt. Soc. Am. B **14**, 1664–1671 (1997).
7. T. J. Kessler, Y. Lin, J. J. Armstrong, and B. Velazquez, "Laser coherence control: technology and applications," in *Laser Coherence Control: Technology and Applications*, H. T. Powell and T. J. Kessler, eds., Proc. SPIE **1870**, 95–104 (1993).
8. Y. Lin, T. J. Kessler, and G. N. Lawrence, "Design of continuous surface-relief phase plates by surface-based simulated annealing to achieve control of focal-plane irradiance," Opt. Lett. **21**, 1703–1705 (1996).
9. Y. Kato, Institute of Laser Engineering, Osaka University, Suita, Osaka, Japan (personal communication, 1984); K. Tsubakimoto, M. Nakatsuka, H. Nakano, T. Kanabe, T. Jitsuno, and S. Nakai, "Suppression of interference speckles produced by a random phase plate, using a polarization control plate," Opt. Commun. **91**, 9–12 (1992); K. Tsubakimoto, T. Jitsuno, N. Miyanaga, M. Nakatsuka, T. Kanabe, and S. Nakai, "Suppression of speckle contrast by using polarization property on second harmonic generation," Opt. Commun. **103**, 185–188 (1993).
10. "Phase conversion using distributed polarization rotation," Laboratory for Laser Energetics (LLE) Review 45, available as NTIS document DOE/DP40200-149 (National Technical Information Service, Springfield, Va., 1990), pp. 1–12; T. E. Gunderman, J.-C. Lee, T. J. Kessler, S. D. Jacobs, D. J. Smith, and S. Skupsky, "Design of continuous surface-relief phase plates by surface-based simulated annealing to achieve control of focal-plane irradiance" in *Conference on Lasers and Electro-Optics*, Vol. 7 of 1990 OSA Technical Digest Series (Optical Society of America, Washington, D.C., 1990), p. 354.
11. T. R. Boehly, V. A. Smalyuk, D. D. Meyerhofer, J. P. Knauer, D. K. Bradley, R. S. Craxton, M. J. Guardalben, S. Skupsky, and T. J. Kessler, "Reduction of laser imprinting using polarization smoothing on a solid-state fusion laser," J. Appl. Phys. **85**, 3444–3447 (1999).
12. J. Paisner, J. D. Boyes, S. A. Kumpan, W. H. Lowdermilk, and M. S. Sorem, "National ignition facility would boost U.S. industrial competitiveness," Laser Focus World, May, 75–77 (1994).
13. M. Desselberger, T. Afshar-rad, F. Khattak, S. Viana, and O. Willi, "Nonuniformity imprint on the ablation surface of laser-irradiated targets," Phys. Rev. Lett. **68**, 1539–1542 (1992); S. G. Glendinning, S. V. Weber, P. Bell, L. B. DaSilva, S. N. Dixit, M. A. Henesian, D. R. Kania, J. D. Kilkenny, H. T. Powell, R. J. Wallace, P. J. Wegner, J. P. Knauer, and C. P. Verdon, "Laser-driven planar Rayleigh–Taylor instability experiments," Phys. Rev. Lett. **69**, 1201–1204 (1992); D. H. Kalantar, M. H. Key, L. B. DaSilva, S. G. Glendinning, J. P. Knauer, B. A. Remington, F. Weber, and S. V. Weber, "Measurement of 0.35-μm laser imprint in a thin Si foil using an x-ray laser backlighter," Phys. Rev. Lett. **76**, 3574–3577 (1996); S. G. Glendinning, S. N. Dixit, B. A. Hammel, D. H. Kalantar, M. H. Key, J. D. Kilkenny, J. P. Knauer, D. M. Pennington, B. A. Remington, R. J. Wallace, and S. V. Weber, "Measurements of laser-speckle-induced perturbations in laser-driven foils," Phys. Rev. E **54**, 4473–4475 (1996); R. J. Taylor, A. L. Velikovich, J. P. Dahlburg, and J. H. Gardner, "Saturation of laser imprint on ablatively driven plastic targets," Phys. Rev. Lett. **79**, 1861–1864 (1997); D. H. Kalantar, M. H. Key, L. B. Da Silva, S. G. Glendinning, B. A. Remington, J. E. Rothenberg, F. Weber, S. V. Weber, E. Wolfrum, N. S. Kim, D. Neely, J. Zhang, J. S. Wark, A. Demir, J. Lin, R. Smith, G. J. Tallents, C. L. S. Lewis, A. MacPhee, J. Warwick, and J. P. Knauer, "Measurements of direct drive laser imprint in thin foils by radiography using x-ray laser backlighter," Phys. Plasmas **4**, 1985–1993 (1997); S. G. Glendinning, S. N. Dixit, B. A. Hammel, D. H. Kalantar, M. H. Key, J. D. Kilkenny, J. P. Knauer, D. M. Pennington, B. A. Remington, J. Rothenberg, R. J. Wallace, and S. V. Weber, "Comparison of drive-seeded modulations in planar foils for 0.35 and 0.53 μm laser drive," Phys. Rev. Lett. **80**, 1904–1907 (1998); T. R. Boehly, V. A. Smalyuk, O. Gotchev, J. P. Knauer, D. D. Meyerhofer, D. K. Bradley, J. A. Delettrez, S. Skupsky, and R. P. J. Town, "The effect of pulse shape and beam smoothing on laser imprinting," Bull. Am. Phys. Soc. **43**, 1664 (1998).
14. R. H. Lehmberg and S. P. Obenschain, "Use of induced spatial incoherence for uniform illumination of laser fusion targets," Opt. Commun. **46**, 27–31 (1983); R. H. Lehmberg, A. J. Schmitt, and S. E. Bodner, "Theory of induced spatial incoherence," J. Appl. Phys. **62**, 2680–2701 (1987); A. V. Deniz, T. Lehecka, R. H. Lehmberg, and S. P. Obenschain, "Comparison between measured and calculated nonuniformities of Nike laser beams smoothed by induced spatial incoherence," Opt. Commun. **147**, 402–410 (1998).
15. T. R. Boehly, D. L. Brown, R. S. Craxton, R. L. Keck, J. P. Knauer, J. H. Kelly, T. J. Kessler, S. A. Kumpan, S. J. Loucks, S. A. Letzring, F. J. Marshall, R. L. McCrory, S. F. B. Morse, W. Seka, J. M. Soures, and C. P. Verdon, "Initial performance results of the OMEGA laser system," Opt. Commun. **133**, 495–506 (1997).
16. D. C. Brown, "High-peak-power Nd:glass laser systems," in *High-Peak-Power Nd:Glass Laser Systems*, D. L. MacAdam, ed., Springer Series in Optical Sciences (Springer-Verlag, Berlin, 1981), Vol. 25, pp. 1–57.
17. "High-frequency bulk phase modulator for broadband

smoothing by spectral dispersion on OMEGA," Laboratory for Laser Energetics (LLE) Review 78, available as NTIS document DOE/SF/19460-295 (National Technical Information Service, Springfield, Va., 1999), pp. 62–81.

18. Photometrics Ltd., Tucson, Ariz. 85706.
19. Color filter glass, Schott Glass Technologies, Inc., Duryea, Pa. 18642.
20. Color filter glass, Hoya Corporation, Tokyo 161-8525, Japan.
21. J. E. Rothenberg, "Two-dimensional beam smoothing by spectral dispersion for direct-drive inertial confinement fusion," in *Solid State Lasers for Application to Inertial Confinement Fusion*, W. F. Krupke, ed., Proc. SPIE **2633**, 634–644 (1995).